SIW-Based Frequency-Tunable Self-Oscillating Active Integrated Antenna

Duo ZHANG [1], Xing CHEN [2], Shishan QI [2], Huili ZHANG [1]

[1] Nanjing Institute of Technology, 211167 Nanjing, China
[2] School of Electronic Engineering and Optoelectronic Technology, Nanjing University of Science and Technology, Xiao Ling Wei 200#, 210094 Nanjing, China

duozhang@njit.edu.cn, qishishan@gmail.com

Submitted November 1, 2022 / Accepted February 13, 2023 / Online first May 5, 2023

Abstract. *A frequency-tunable self-oscillating active integrated antenna (AIA) mainly composed of active circuit and 1×2 substrate integrated waveguide (SIW) antenna array is proposed in this paper. Manipulating bias voltage to the varactors loaded on SIW antenna could offer electronic control of oscillation frequency. The DC bias circuit of the varactors integrated in SIW cavity can provide compact structure. Due to the load effect of the high Q SIW cavity, the designed antenna exhibits low phase noise. According to the measured results, the effective isotropic radiated power (EIRP) ranges from 4.4 to 12.9 dBm which is superior to previous reports with the frequency tuning range of about 20 MHz. The phase noise is −92.7 dBc/Hz at 100 kHz offset. The measured results also show that the cross-polarization levels are almost 20 dB lower than the co-polarized one in the main beam direction at 5.698 GHz.*

Keywords

Substrate Integrated Waveguide (SIW), Active Integrated Antenna (AIA)

1. Introduction

The self-oscillating active integrated antenna (SOAIA), integration of oscillation circuit and passive radiator, shows superiority in achieving compact and low-cost unmodulated RF sources in wireless power transmission system. The SOAIAs find applications in multicarrier radio frequency identification (RFID) and Internet of Things systems (IoT) [1–3]. With the increasing demands of reliable communication link, the extension of readable range has become one of the research hotspots in recent years [4]. SOAIAs with the flexibility of operating frequency rise in response to the proper time and conditions.

It is regrettable that there are few reports on SOAIAs with frequency tunability in recent years, so we discuss the only remaining relevant reports. Embedding transistors and varactors into the ring or semi-ring antenna provides a compact way to develop frequency-tunable SOAIA along with good phase noise, since it is based on the feedback loop method [5–7]. SIW antenna with planar structure is easy to integrate with active circuits, and it can be used to design SOAIA [8–10]. The latest research about frequency-tunable SOAIA is proposed by Moitreya Adhikary [10]. He proposed a SIW-based SOAIA with automated beam scanning function, and we can also find frequency tunability in this work. With the oscillator section designed by negative resistance oscillation principle, the antenna in [10] acts more as a reactive load, which causes a larger size. As SOAIA integrates more and more electronic switches to achieve multiple functions, it is important to find ways to reduce the size. By utilizing SIW structure, the cathodes of switches can be soldered to the metal surfaces of SIW and connected to the ground terminal with a DC power supply [11]. In this way, the bias circuit in SOAIAs, especially in those work focusing on multi-dimensional reconfigurability, can be simplified and integrated inside the SIW cavity. The bias circuit of positive voltage can be constructed on the bottom layer of the SIW cavity, which avoids soldering DC wires on the radiating top surface, thereby minimizing their influence on radiation performance [12]. From our point of view, it is a potential way to design compact SOAIAs.

In this paper, a SIW-based frequency-tunable SOAIA is proposed as shown in Fig. 1. The proposed SOAIA is designed by field-circuit co-simulation based on multi-port scattering parameters. A 2×1 SIW antenna array for improving EIRP is placed in the feedback loop of oscillator. Frequency-tunability is realized by changing the bias voltage of the varactors loaded on the SIW antenna. The cathodes of varactors are soldered to the top layer of SIW and the bias circuit of anodes is constructed on the bottom layer. The measured results show that the proposed AIA features its high EIRP with the reduced tuning bandwidth. The phase noise, figure of merit (FOM) and efficiency (η) are measured and calculated at 5.698 GHz, and these performances are also very competitive when compared with current SOAIAs operating at single frequency [3], [13].

DOI: 10.13164/re.2023.0221

2. Active Circuit and Antenna Design

2.1 Active Circuit Design

The proposed SOAIA is designed to work in C-band referring to the operating band of RFID and IoT. It is formed on a single dielectric substrate (Rogers RO4003c, $\varepsilon_r = 3.55$, $\tan\delta = 0.0027$, $h = 0.813$ mm) with double layer coppers. The active circuit provides gain compensation for the losses of antenna to start and maintain the oscillation. The SIW antenna array serves as both a passive resonator contributing to the oscillation and a radiator with improved EIRP. In order to obtain the performance of active part and antenna in the simulation operated in ADS and HFSS respectively, microstrip line has been broken and port P_1 and P_2 are assigned at the breakpoints as shown in Fig. 1(a). S-parameters of SIW antenna array are imported in ADS as a data item to perform a field-circuit co-simulation to find oscillation parameters.

The transistor, BFP520, is biased at $V_B = 0.9$ V, $V_C = 2$ V, and $I_C = 15$ mA. Two resistors, $R_b = 15$ kΩ, and $R_c = 68$ Ω, are connected in parallel using $V_{BJT} = 3$ V. The fan-shaped stub and 100 Ω microstrip line serve as the radio frequency chock (RFC). Those works, which had been done in [14], are mainly focused on the low phase

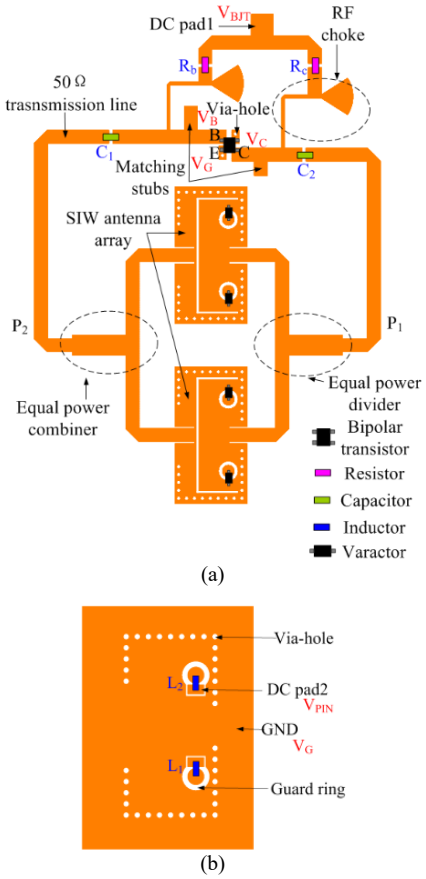

Fig. 1. Layout and geometry of the proposed voltage-controlled AIA. (a) Top layer. (b) One part of bottom layer.

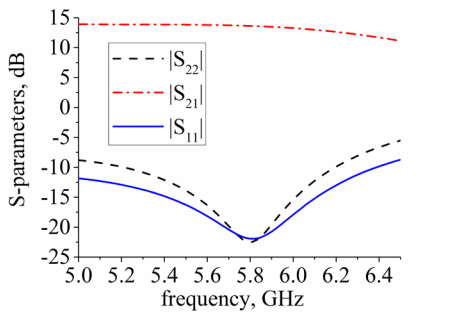

Fig. 2. Simulated S-parameter of the transistor.

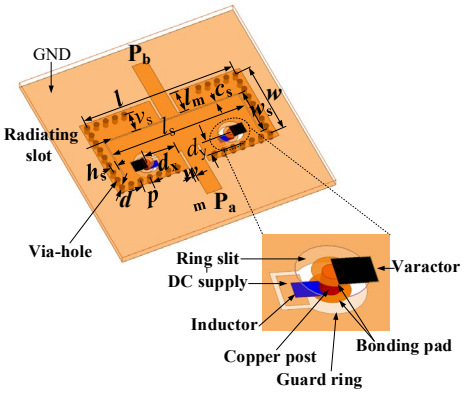

Fig. 3. Configuration of the frequency tunable SIW antenna. Design dimensions are (in mm): $l = 17.6$, $w = 8.8$, $l_m = 3$, $w_m = 0.3$, $l_s = 15.76$, $w_s = 5.62$, $c_s = 0.12$, $h_s = 0.8$, $v_s = 2.5$, $d_x = 3.8$, $d_y = 1.9$, $d = 0.6$, $p = 1.1$.

noise performance and could be seen as the starting point of this design. The biased unstable transistor can provide gain around 13 dB as Figure 2 shows.

2.2 Frequency-Tunable SIW Antenna Design

The configuration of the proposed SIW antenna element is shown in Fig. 3. In the condition that the increased size of radiator will increase the overall area of oscillator, the U-shaped radiating slot is used to reduce the SIW antenna size [15]. The antenna is fed by 50 Ω coplanar waveguide connected with the transmission line at port P_a and P_b.

A pair of ring slits are etched symmetrically on the top layer of the SIW antenna for placing the varactors, Skyworks SMV2023-011LF. The rings etched on the bottom layer are used to provide isolation between the ground potential $V_G = 0$ V and the positive voltage V_{PIN} that drives the varactor through the metallized holes. The inductors, $L_1 = L_2 = 47$ nH serve as RFC.

As shown in Fig. 1(a), two designed SIW antenna elements are placed with the interval of half wavelength, which forms a 1 × 2 array to realize in-phase current addition. T-shaped microstrip structure is used for equal power division and combination at the collector side and the base side respectively. The inductors and varactors are modeled as the 0.8 mm × 0.6 mm and 1.52 mm × 1.37 mm rectangular patch with lumped RLC boundary respectively according

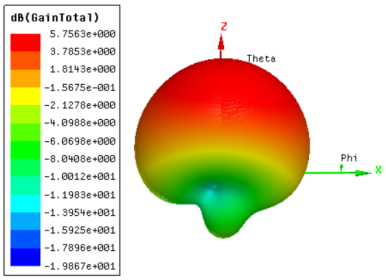

Fig. 4. Simulated radiation pattern at 5.698 GHz.

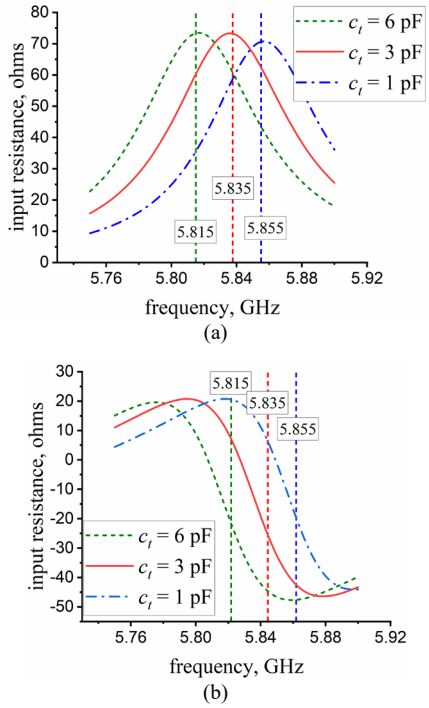

Fig. 5. Simulated input resistance of voltage-controlled SIW antenna array with loaded capacitor of 1 pF, 3 pF and 6 pF: (a) Real part of impedance. (b) Imaginary part of impedance.

to their datasheets. Port P_1 and P_2 are set as lumped port of 50 Ω with the excitation of 1 ∠ 0°and 1 ∠ 108° in HFSS to simulate the oscillation situation, and the radiation gain G_t is estimated to be 5.76 dB at 5.698 GHz as Figure 4 shows.

The simulated input resistance of the antenna array loaded with different capacitor (c_t = 6 pF, 3 pF, and 1 pF) is shown in Fig. 5. It can be inferred that the resonant frequency of SIW antenna will move steadily downward to the lower frequency side as the capacitance of the varactor increases. The reverse capacitance of the varactor changes with the bias voltage V_{PIN}, thus the resonant frequency of designed SIW antenna is voltage-controlled.

2.3 Oscillation Parameters Analysis

Two-port S-parameters of SIW antenna array are imported in ADS as a data item to perform a co-simulation with the active circuit. An oscillator test probe is placed between port P_1 and P_2 to check the oscillation. To start and

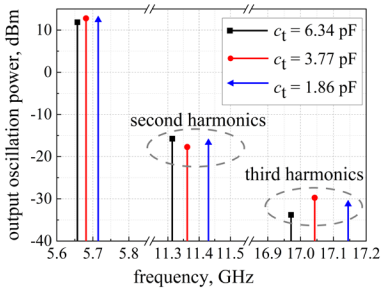

Fig. 6. Simulated oscillation power spectra of the proposed voltage-controlled AIA with loaded capacitor of 6.34 pF, 3.77 pF, and 1.86 pF.

and maintain the oscillation, Equation (1) must be satisfied, which is:

$$\begin{cases} \left|G_{BJT}(jw_0)\right|^2 \left|L_{ANT}(jw_0)^2\right| \geq 1, \\ \angle\left|G_{BJT}(jw_0)L_{ANT}(jw_0)\right| = 2n\pi, \ n = 0,1,2\cdots \end{cases} \tag{1}$$

where G_{BJT}, L_{ANT}, and w_0 are the voltage gain of the common-emitter transistor, the loss of the antenna and the oscillation angular frequency, respectively.

With each capacitance value that varactor SMV2023-011LF provides (eg. 6.34 pF, 3.77 pF, and 1.86 pF), the closed loop has the phase delay of 0° and the loop-gain greater than 1 satisfying the oscillation starting condition. The output oscillation power P_t are respectively 11.87 dBm, 12.78 dBm, and 12.41 dBm, and the second harmonics are at least 26 dB below the fundamental one as Figure 6 shows.

3. Experimental Validation and Discussion

The fabricated frequency-tunable AIA is shown in Fig. 7. The total size is 78 mm × 85 mm. The reverse current of varactor is almost 0 A, thus the DC power consumption of it can be ignored. The total DC power consumption is 14.7 dBm. The emission characteristics are measured by using a standard horn antenna connected to a spectrum analyzer to receive the radiated power of AIA.

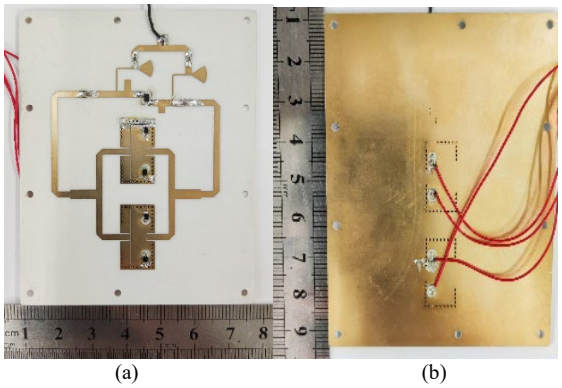

Fig. 7. Fabricated voltage-controlled AIA. (a) Top layer. (b) Bottom layer.

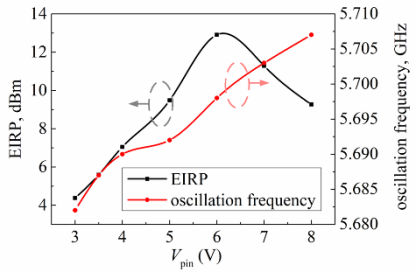

Fig. 8. Measured oscillation frequency and EIRP of the AIA versus the reversed bias of the varactor.

The separation between the AIA and horn antenna is 5.3 m to guarantee the required far-field condition. The loss of the connecting cable is 1 dB and the gain of horn antenna is about 14.9 dBi around 5.7 GHz.

By increasing the reverse bias voltage of the varactor or equivalently decreasing the junction capacitance, the measured oscillation frequency and EIRP are illustrated in Fig. 8. EIRP is computed:

$$EIRP = P_{t(dB)} + G_{t(dB)} = P_{r(dB)} - G_{r(dB)} - L_{r(dB)} - 20\log\left(\frac{\lambda_0}{4\pi R}\right) \quad (2)$$

where P_t, G_t, P_r, G_r, L_r, R, and λ_0 are the output power of oscillator (dBm), gain of AIA (dB), radiated power of AIA (dBm), gain of receiving antenna (dB), loss of the connecting cable (dB), separation between the AIA and receiving antenna and wavelength in free space.

The oscillation frequency steadily increases as the bias voltage increases. The EIRP ranges from 4.4 to 12.9 dBm with the bandwidth of 20 MHz. Difference in output levels can be accounted for the gain difference of SOAIA and receiving antenna at varied frequencies, as well as the parasitic loss of the varactors. Since EIRP of the design is 12.91 dBm at 5.698 GHz, the oscillation output power P_t of the active antenna can be calculated from (2) as 7.21 dBm, which is slightly lower than the simulation result in Fig. 6, and the calculated η is 17.5%.

The measured phase noise is −92.7 dBc/Hz at 100 kHz offset 5.698 GHz as Figure 9 shows. EIRP and phase noise are included to determine the FOM, thus the FOM can evaluate the general performance of oscillator, which is calculated to be −185.3 dBc/Hz in this work. Radiation patterns in E-plane and H-plane are measured at 5.698 GHz in the far-field region and plotted after normalizing the recorded data to their maximum values as Figure 10 shows. The main beam radiation is along the +z-axis and the cross-polarization levels are almost 20 dB lower than the co-polarized ones in the main beam direction.

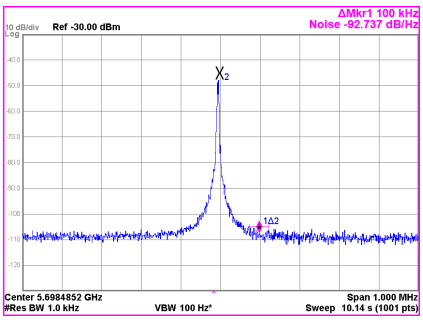

Fig. 9. Measured phase noise at 100 kHz, offset 5.698 GHz.

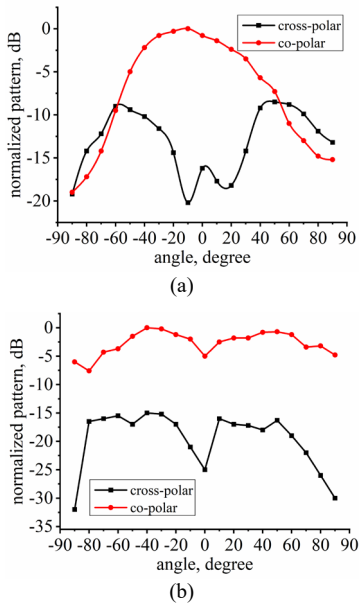

Fig. 10. Measured radiation pattern normalized to its maximum. (a) E-plane. (b) H-plane.

Ref.	Operating frequency (GHz)	EIRP (dBm)	η P_t/P_{dc} (%)	Phase noise @100 kHz offset (dBc/Hz)	FOM @100 kHz offset (dBc/Hz)
[5]	4.270–4.940 (state 1)	8.2–9.1	28.3@4.6G	−88.0*	−177.1*
[7]	4.470–4.850 (off state)	8.0–9.0*	12.4@4.72G	−74.3	−161.2*
[10]	10.500–10.950	around 0	around 1.4	NA**	NA**
[3]	0.916	7.0	19.3	−108.5 @1 MHz offset	−182.5* @1 MHz offset
[13]	0.920	8.9	52.0	−94.0*	−170.7*
This	5.682–5.707	4.4–12.9	17.5@5.698G	−92.7	−185.3

Note:* Calculated/Estimated from the data given in literature. **NA: not reported in literature.

Tab. 1. Comparison of the performances of various SOAIAs.

The performance of the reported self-oscillation AIA along with those of this work are encapsulated in Tab. 1. The measured results show the superiority of the proposed AIA in many indicators.

4. Conclusion

With the aid of varactors loaded on SIW antenna, a new self-oscillating AIA with frequency tunability has been developed and experimentally verified. The proposed

frequency-tunable AIA shows improved EIRP with simple structure. According to the experimental results, this work also demonstrates low phase noise and excellent FOM, which is competitive as a low-cost unmodulated continuous wave charging source.

Acknowledgments

This work was funded by projects including the Scientific Research Foundation for the Highlevel Personnel of Nanjing Institute of Technology (grant: YKJ2019109 and YKJ2019108).

References

[1] ADHIKARY, M., BISWAS, A., AKHTAR, M. J. Active integrated antenna based permittivity sensing tag. *IEEE Sensors Letters*, 2017, vol. 1, no. 6, p. 1–4. DOI: 10.1109/LSENS.2017.2768560

[2] SHARAWI, M. S., HAMMI, O. *Design and Applications of Active Integrated Antennas.* London (UK): Artech House, 2018. ISBN: 9781630813581

[3] TSAI, Y. L., CHU, H. N., MA, T. G. Self-oscillating circularly polarized active integrated monopole antenna using cross-coupled pair and inverted-l strip. *IEEE Antennas and Wireless Propagation Letters,* 2020, vol. 19, no. 7, p. 1132–1136. DOI: 10.1109/LAWP.2020.2991467

[4] LIN, Y. Y., MA, T. G. Frequency-reconfigurable self-oscillating active antenna with gap-loaded ring radiator. *IEEE Antennas and Wireless Propagation Letters*, 2013, vol. 12, p. 337–340. DOI: 10.1109/LAWP.2013.2250475

[5] WU, C. H., MA, T. G. Pattern-reconfigurable self-oscillating active integrated antenna with frequency agility. *IEEE Transactions on Antennas and Propagation,* 2014, vol. 62, no. 12, p. 5992–5999. DOI: 10.1109/TAP.2014.2361897

[6] LIN, Y. Y., WU, C. H., MA, T. G. Miniaturized self-oscillating annular ring active integrated antennas. *IEEE Transactions on Antennas and Propagation*, 2011, vol. 59, no. 10, p. 3597–3606. DOI: 10.1109/TAP.2011.2163782

[7] WU, C. H., MA, T. G. Self-oscillating semi-ring active integrated antenna with frequency reconfigurability and voltage-controllability. *IEEE Transactions on Antennas and Propagation*, 2013, vol. 61, no. 7, p. 3880–3885. DOI: 10.1109/TAP.2013.2256095

[8] ADHIKARY, M., SAHOO, S. K., BISWAS, A., et al. SIW-based self-oscillating concurrent dual-frequency active integrated antenna. *IEEE Antennas and Wireless Propagation Letters*, 2019, vol. 18, no. 9, p. 1897–1901. DOI: 10.1109/LAWP.2019.2932498

[9] GIUPPI, F., GEORGIADIS, A., COLLADO, A., et al. A compact, single-layer substrate integrated waveguide (SIW) cavity-backed active antenna oscillator. *IEEE Antennas and Wireless Propagation Letters,* 2012, vol. 11, p. 431–433. DOI: 10.1109/LAWP.2012.2194470

[10] ADHIKARY, M., SARKAR, A., SAHOO, S. K., et al. Half-mode SIW based active integrated circularly polarized leaky wave antenna for automated beam scanning applications. In *Proceedings of 2019 IEEE MTT-S International Microwave and RF Conference (IMARC)*. Mumbai (India), 2019, p. 1–4. DOI: 10.1109/IMaRC45935.2019.9118685

[11] GE, L., LI, Y., WANG, J., et al. A low-profile reconfigurable cavity-backed slot antenna with frequency, polarization, and radiation pattern agility. *IEEE Transactions on Antennas and Propagation,* 2017, vol. 65, no. 5, p. 2182–2189. DOI: 10.1109/TAP.2017.2681432

[12] JI, Y., GE, L., WANG, J., et al. Simple beam scanning SIW cavity-backed slot antenna using postloaded varactor. *IEEE Antennas and Wireless Propagation Letters*, 2019, vol. 18, no. 12, p. 2761–2765. DOI: 10.1109/LAWP.2019.2951447

[13] CHANG, Y. W., MA, T. G. Zeroth-order self-oscillating active integrated antenna using cross-coupled pair. *IEEE Transactions on Antennas and Propagation*, 2017, vol. 65, no. 10, p. 5011–5018. DOI: 10.1109/TAP.2017.2735486

[14] CHEN, X., QI, S. S., CHEN, S. L., et al. A low phase noise self-oscillating active antenna. In *Proceedings of 2021 International Conference on Microwave and Millimeter Wave Technology (ICMMT).* Nanjing (China), 2021, p. 1–3. DOI: 10.1109/ICMMT52847.2021.9618470

[15] ASTUTI, D. W., RAHARDJO, E. T. Size reduction of substrate integrated waveguide cavity backed u-slot antenna. In *Proceedings of 2018 IEEE Indian Conference on Antennas and Propagation (InCAP)*. Hyderabad (India), 2018, p. 1–4. DOI: 10.1109/INCAP.2018.8770702

About the Authors ...

Duo ZHANG received the Ph.D. degree in Microwave Engineering from the Nanjing University of Science & Technology in 2018. Currently, he is working at the Nanjing Institute of Technology from 2019. His research interests include microwave circuit design and radar system research.

Xing CHEN received the Master degree in Electromagnetic Field and Microwave Technology from the Nanjing University of Science & Technology in 2022. His research interests include microwave circuit design and antenna theory.

Shishan QI (corresponding author) received the Ph.D. degree in Electromagnetic Field and Microwave Technology from the Nanjing University of Science & Technology in 2012. Currently, he is working at the Nanjing University of Science & Technology from 2012. His research interests include microwave antenna theory and radar system research.

Huili ZHANG received the Ph.D. degree in Radio Physics from the Nanjing University in 2019. Currently, she is working at the Nanjing Institute of Technology from 2019. Her research interests include microwave circuit design and superconducting electronics research.